

Bahaviors of Ca II K line in A-type stars

Yoichi TAKEDA

11-2 Enomachi, Naka-ku, Hiroshima-shi, 730-0851, Japan
 ytakeda@js2.so-net.ne.jp

(Received 2020 October 31; accepted 2020 November 23)

Abstract

A synthetic spectrum-fitting analysis was applied to the resonance Ca II line at 3933.68 Å for a large sample of 122 A-type main-sequence stars ($7000 \lesssim T_{\text{eff}} \lesssim 10000$ K) in a wide range of projected rotational velocity ($10 \lesssim v \sin i \lesssim 300$ km s^{−1}), with an aim of investigating the behaviors of Ca abundances ($[\text{Ca}/\text{H}]_{39}$) determined from this strong Ca II 3934 line, especially in context of (i) how they are related with the Am phenomenon (often seen in slow rotators) and (ii) whether they are consistent with the Ca abundances ($[\text{Ca}/\text{H}]_{61}$) previously derived by the author from the weaker Ca I 8162 line. It was confirmed that Ca line strengths in Am stars tend to be weaker and associated abundances are lower compared to non-Am stars at the same T_{eff} , indicating a deficiency of Ca in the photosphere of Am stars. However, an appreciable fraction of cool Am stars ($T_{\text{eff}} \lesssim 8000$ K) were found to show extraordinarily anomalous Ca II 3934 line feature (i.e., unusually broad for its considerable weakness) which is hard to explain. Regarding the comparison between $[\text{Ca}/\text{H}]_{39}$ and $[\text{Ca}/\text{H}]_{61}$, while both are roughly consistent with each other for hotter stars ($T_{\text{eff}} \gtrsim 8000$ K), the former tends to be lower (by up to ~ 1 dex or even more) than the latter for cooler A stars ($T_{\text{eff}} \lesssim 8000$ K) including those “weak broad K line” objects. This fact suggests that some special mechanism reducing the strength of Ca II 3934 line is involved at $T_{\text{eff}} \lesssim 8000$ K where $[\text{Ca}/\text{H}]_{39}$ would be no more reliable. Whereas atomic diffusion causing the deficit of Ca in the photosphere as a result of element segregation in the deeper radiative envelope may be regarded as a promising explanation because it seems to fit in the qualitative trend of $[\text{Ca}/\text{H}]_{61}$ in A-type stars, the well-known feature of considerably weak Ca II K line in classical Am stars should not necessarily be attributed to only this element diffusion scenario, for which some unknown weakening mechanism specific to this resonance line may independently be operative.

Key words: stars: abundances — stars: atmospheres — stars: chemically peculiar — stars: early-type — stars: rotation

1. Introduction

The resonance line of once-ionized calcium at 3933.68 Å (multiplet 1, historically designated as “K”), manifestly standing out in the violet region of the spectrum, is so strong as to be visible in most stars from K through B type and is regarded as one of the most important lines in stellar spectroscopy. In context of early-type stars, this Ca II K line is known to play a significant role in the spectral classification of chemically-peculiar stars, especially with regard to metallic-lined A-type stars (hereinafter called Am stars), which occupy an appreciable fraction (~ 10 – 20%) of A stars and are generally slower rotators ($v \sin i \lesssim 100$ km s^{−1}) characterized by strong metallic lines (e.g., those of Fe group elements). That is, A-type stars are classified as Am, when three spectral types judged from Ca II K line, H I (Balmer) lines, and metallic lines are discrepant with each other as $\text{Sp}(K) < \text{Sp}(H) < \text{Sp}(\text{Metal})$; i.e., Ca II K line is weaker (indicating earlier type) while metallic lines are stronger (indicating later type) compared to the spectral type from

the Balmer lines (good metallicity-free indicator of T_{eff}).

While such conspicuous weakness of Ca II K line in Am stars was a matter of debate at first, it has become generally considered to be due to deficit of Ca in the atmosphere since the advent of diffusion theory in 1970s (e.g., Watson 1971; Smith 1973). That is, gravitational settling may take place in the deeper radiative envelope (possibly stable in slow rotators free from significant mixing), which would eventually yield surface underabundance of Ca (see, e.g., Richer et al. 2000 or Talon et al. 2006 and the references therein for more recent theoretical calculations).

Actually, most chemical abundance studies on Am stars so far have shown the existence of an appreciable deficiency in Ca (along with Sc, another element showing weak lines in Am stars) by several tenths dex to ~ 1 dex (e.g., Conti 1970, Varenne & Monier 1999, Hui-Bon-Hoa 2000, to mention a few). Quantitatively speaking, however, the extent of Ca abundance anomaly with regard to Am phenomena is rather diversified depending on each investigation; for example, Gebran et al. (2010) reported

that Ca in Hyades Am stars is not so much deficient but even almost normal (cf. figure 5b therein).

Here, it should be pointed out that almost all these Ca abundance studies have been done by using lines of neutral calcium (a number of such Ca I lines are available in 4200–6500 Å region; see, e.g., table 2 in Conti 1965). In contrast, systematic abundance investigations based on Ca II 3934 line for a large sample of upper main-sequence stars have rarely been done so far, which is presumably due to the considerable difficulty in precisely measuring the strength of this line with appreciable damping wings under the influence of blending with neighboring lines. Nevertheless, the following studies that investigated the Ca abundance trends for a number of A-type stars based on the Ca II K line are worth mentioning.

- Henry (1969) carried out narrow-band photometric observations of Ca II 3934 line (k index) for an extensive sample of 146 A-type stars and investigated the strengths of this line. He found that the Ca abundances of sharp-line stars vary by a factor of ~ 2 and (somewhat surprisingly) that a substantial fraction of Am stars have normal K-line strengths.
- Guthrie (1987) derived the equivalent widths of Ca II 3934 line for 57 Am stars mainly based on the published k indices or K-line spectral types taken from various literature, and determined their Ca abundances, which showed a large dispersion but were generally underabundant relative to the Sun ($-1 \lesssim [\text{Ca}/\text{H}] \lesssim 0$). The deficiency appeared to have some correlation with age (i.e., position on the HR diagram), which he suggested may be consistent with the diffusion theory.
- North et al. (1997), in their study of absolute magnitude of chemically peculiar stars, mentioned their Ca abundance determinations for 27 Am stars from the Ca II K line by using the spectrum synthesis method based on their high-dispersion spectroscopic observations. Since their abundances were in good agreement with Guthrie's (1987) results for 8 stars in common, they combined both to make a large data sample of 76 Am stars, from which they found a T_{eff} -dependence of Ca abundances (i.e., deficiency tends to be more enhanced towards lower T_{eff}). Unfortunately, they neither gave any account about the procedure of their spectrum synthesis analysis nor detailed abundance results for scrutiny.

As such, comprehensive Ca abundance studies of A and Am stars based on the Ca II K line of ionized calcium are few in number, despite that several investigations using Ca I lines of neutral calcium using high-quality are already available. Given that suspicion existed in the past (e.g., Böhm-Vitense 1976, 2006) that the weakness of Ca II K line in Am stars might be due to unusual atmospheric condition (e.g., anomalous ionization) rather than the abundance effect, careful analysis of the Ca II 3934 line on a large sample of A-type stars would be in order and worthwhile.

About a decade ago, Takeda et al. (2009; here-

inafter referred to as Paper I) conducted Na abundance determinations based on the synthetic spectrum fitting method applied to the 5880–5905 Å region comprising Na I 5890/5896 doublet (D) for 122 A-type stars of slow as well as rapid rotators ($10 \lesssim v \sin i \lesssim 300 \text{ km s}^{-1}$). Ca abundances (along with those of O, Fe, Si, and Ba) were also determined for these sample stars, since a supplementary spectrum fitting analysis was likewise carried out in that study on the 6140–6170 Å region (for the purpose of determining $v \sin i$ and abundances of important key elements) which comprises Ca I lines (among which the strongest is the Ca I 6162.17 line of multiplet 3). Fortunately, thanks to the wide wavelength coverage (~ 3700 – 10000 Å) of the echelle spectra employed in Paper I, they can be used also for the analysis of Ca II 3934 line of present interest.

Accordingly, the author thought about conducting Ca abundance determinations from the Ca II K line for these 122 stars based on the similar spectrum fitting analysis applied to the observational data used in Paper I, while placing the main focus on the following questions: (i) How are the Ca abundances established from the Ca II K line related with Am phenomenon? Is there a distinct difference between normal A stars and Am stars in this respect? (ii) Are the Ca abundances derived from the Ca I 6162 line in Paper I and those from the Ca II 3934 line consistent with each other? This comparison may serve for checking the usability of Ca II K line as an abundance indicator. To clarify these points was the purpose of this investigation.

2. Observational data

The program stars of this study are 122 apparently bright ($V \lesssim 6$) A-type main-sequence stars, which are listed in table 1. The basic observational data of these targets are the echelle spectra (with a spectral resolution of $R \sim 45000$) widely covering the wavelength range from ~ 3700 Å to ~ 10000 Å, which were obtained in 2008 January, 2008 September, and 2009 January by using BOES (Bohyunsan Observatory Echelle Spectrograph) attached to the 1.8 m reflector at Bohyunsan Optical Astronomy Observatory. See section 2 in Paper I for more details regarding the observations and data reduction. Due to the lowered sensitivity of the CCD detector in the violet region, the S/N ratio around the Ca II 3934 line of present interest is not so high (from several tens to ~ 100 – 200 differing from star to star) as compared to the yellow–red region. The violet-region spectrum of Procyon, which was employed as the standard reference star, was adopted from the UVES-POP database (Bagnulo et al. 2003).¹

3. Stellar parameters

Regarding the fundamental atmospheric parameters of 122 program stars, the same values as used in Paper I were adopted (see subsection 3.1 therein for more details): The effective temperature (T_{eff}) and the surface

¹ http://www.eso.org/sci/observing/tools/uvespop/bright_stars_uptonow.html

gravity ($\log g$) were determined photometrically mainly from Strömberg’s $uvby\beta$ colors according to Napiwotzki et al.’s (1993) calibration, while the microturbulence (v_t) was derived from T_{eff} by using Takeda et al.’s (2008) empirical formula. These parameters are summarized in table 1. Among the 122 sample stars, 28 are metallic-lined A-type (Am) stars, which are classified as Am in (at least one of) the published spectral classifications compiled in the SIMBAD database (cf. column 16 in table 1). As in Paper I, Kurucz’s (1993) solar-metallicity model-atmosphere grid was used to be interpolated in terms of T_{eff} and $\log g$ for each star. Regarding Procyon, the same atmospheric parameters and model atmosphere as adopted in Paper I were used (cf. section IV(c) in Takeda et al. 2008).

4. Spectrum fitting analysis

4.1. Outline of the method

The procedures of abundance determination are essentially the same as in Paper I (cf. section 4 therein). First, by applying the numerical algorithm described in Takeda (1995), the best fit between the synthetic and observed spectra was accomplished in the specified wavelength region while varying the abundances of important elements (A_1, A_2, \dots), $v \sin i$ (projected rotational velocity), and $\Delta\lambda$ (radial velocity or wavelength shift). Then, the equivalent width (W) of the relevant line of interest (Ca in the present case) was “inversely” evaluated from the best-fit abundance solution with the same atmospheric model/parameters as used in the spectrum-fitting analysis. This W was further used to estimate the abundance uncertainties due to ambiguities of atmospheric parameters by perturbing the standard values interchangeably. Theoretical line-formation calculations (necessary for spectrum synthesis or for evaluation of W) were made under the assumption of LTE (Local Thermodynamic Equilibrium) throughout this study, since the non-LTE effect is likely to be insignificant for the relevant Ca lines (see appendix 1).

4.2. Analysis of Ca I 6162 and Ca II 3934 lines

This spectrum fitting for the 6140–6170 Å region comprising Ca I lines was already done in Paper I, where the atomic parameters of all spectral lines were taken from Kurucz and Bell’s (1995) compilation and the abundances of five elements (O, Si, Ca, Fe, and Ba) were varied. Hereinafter, the quantities derived from the fitting analysis in this wavelength region are denoted with suffix “61”. How the theoretical spectrum for the converged parameters fit the observed spectrum is demonstrated in figure 2 of Paper I, and the resulting $A_{61}(\text{Ca})$ and $v \sin i_{61}$ for each star are presented in table 1. Among the several Ca I lines of appreciable strengths included in this 6140–6170 Å region, the main focus is placed on the strongest Ca I 6162.17 line (multiplet 3, $\chi_{\text{low}} = 1.90$ eV; see table 2 for the atomic parameters of this line). Therefore, the

equivalent widths of this Ca I 6162 line (W_{61}) were calculated inversely from $A_{61}(\text{Ca})$, which are also given in table 1.

Similarly, in order for the main purpose of determining the Ca abundance from the strong Ca II 3934 line, synthetic spectrum fitting analysis was done in the same manner for the 3910–3955 Å region, where the atomic parameters were taken from the VALD database (Ryabchikova et al. 2015) and the abundances of Ca and Fe were varied. The quantities derived from this 3910–3955 Å fitting are denoted with suffix “39”. The resulting solutions of $A_{39}(\text{Ca})$ and $v \sin i_{39}$ for each star are given in table 1, while the theoretical spectrum for the converged parameters is compared with the observed spectrum is displayed for each star in figure 1. Likewise, the equivalent widths (W_{39}) of the Ca II 3933.68 line (multiplet 1, $\chi_{\text{low}} = 0.00$ eV; see table 2 for the adopted atomic parameters) were evaluated inversely from $A_{39}(\text{Ca})$ and are listed in table 1.

The equivalent widths, Ca abundances, and their sensitivities to perturbations of atmospheric parameters (T_{eff} , $\log g$, and v_t) estimated in the same manner as in Paper I (see the caption in figure 2 of this paper) are plotted against T_{eff} in figure 2 (Ca I 6162) and figure 3 (Ca II 3934).

5. Discussion

5.1. Trend of Ca line strengths

It may be worthwhile to examine the behaviors of the Ca I 6162 and Ca II 3934 lines from the viewpoint of the parameter dependence. As can be seen from figure 2a and figure 3a, W_{61} as well as W_{39} are progressively weakened with an increase in T_{eff} , the gradient being especially steeper for the former. This may be interpreted as the T_{eff} -dependence of the number population of the lower level from which the line forms.

According to the Saha–Boltzmann equation, the T -dependence for the number population (n_i^m) of level i ($i = 0$ for the ground level) at ionization stage m (=I, II, III) can be expressed as

$$n_i^m \propto n_0^{m+1} \exp[(\chi_{\text{ION}}^m - \chi_i^m)/(kT)] \quad (1)$$

and

$$n_i^m \propto n_0^m \exp[-\chi_i^m/(kT)] \quad (2)$$

where χ_i^m is the excitation potential of level i at ionization stage m , χ_{ION}^m is the ionization potential (from the ground level of ionization stage m), and k is the Boltzmann constant (note that the T -dependent term proportional to $\propto T^{-3/2}$ was neglected in equation (1) because it is insignificant compared to the exponential term). Then, n_i^{I} and n_i^{II} can be written in terms of n_0^{III} as

$$n_i^{\text{I}} \propto n_0^{\text{III}} \exp[(\chi_{\text{ION}}^{\text{I}} + \chi_{\text{ION}}^{\text{II}} - \chi_i^{\text{I}})/(kT)] \quad (3)$$

and

$$n_i^{\text{II}} \propto n_0^{\text{III}} \exp[(\chi_{\text{ION}}^{\text{II}} - \chi_i^{\text{II}})/(kT)]. \quad (4)$$

Here, the important point is that Ca is mainly in the twice-ionized stage (Ca III) in the photosphere ($\tau_{5000} \sim$

² Abundances of the remaining elements were fixed.

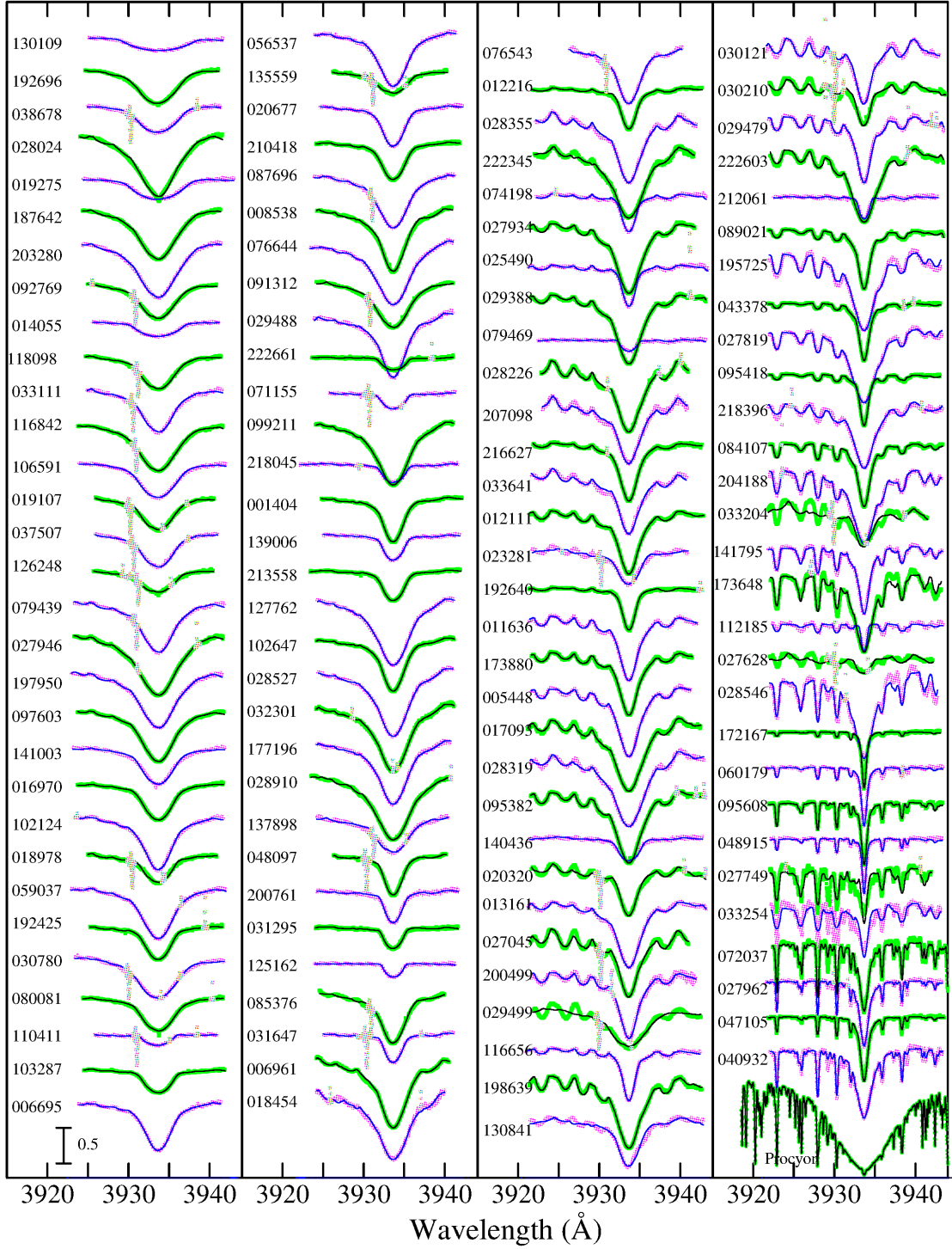


Fig. 1. Synthetic spectrum fitting at the 3910–3955 Å region (comprising the Ca II 3934 line) accomplished by varying the projected rotational velocity ($v_e \sin i_{39}$) along with the abundances of Ca and Fe. The best-fit theoretical spectra are shown by black/blue solid lines, while the observed data are plotted by green/pink symbols (note that the masked portions of the observed spectra which were discarded because of the spectrum defect are indicated by gray symbols). In each panel, the spectra are arranged in the descending order of $v_e \sin i_{61}$ as in table 1, and an offset of 0.5 is applied to each spectrum (indicated by the HD number, where that of “Weak Broad K-line” star is colored in red) relative to the adjacent one. The case of Procyon (standard star) is displayed at the bottom of the rightmost panel.

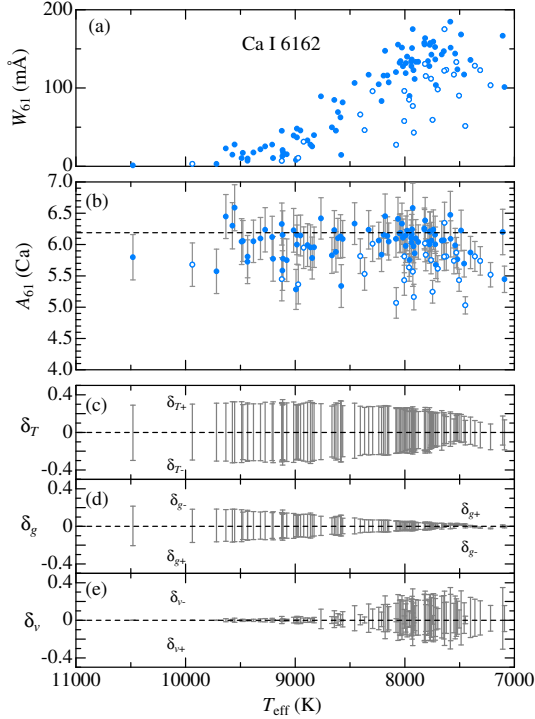


Fig. 2. Abundance-related results derived from 6140–6170 Å fitting (comprising Ca I lines) plotted against T_{eff} . (a) Equivalent width of Ca I 6162 line (W_{61}), (b) $A_{61}(\text{Ca})$ (logarithmic number abundance of Ca in the usual normalization of $A_{\text{H}} = 12.00$), (c) δ_{T+} and δ_{T-} (Ca abundance variations in response to T_{eff} changes of +300 K and −300 K), (d) δ_{g+} and δ_{g-} (Ca abundance variations in response to $\log g$ changes of +0.3 dex and −0.3 dex), and (e) δ_{v+} and δ_{v-} (abundance variations in response to changing v_t as $v_t \times 1.3$ and $v_t/1.3$). In panels (a) and (b), Am stars (see the remark in table 1) are expressed in open symbols. The error bars attached in the symbols in panel (b) are $\delta_{T_{\text{eff}}} \equiv \sqrt{\delta_{T+}^2 + \delta_{T-}^2}$, where $\delta_T \equiv (|\delta_{T+}| + |\delta_{T-}|)/2$, $\delta_g \equiv (|\delta_{g+}| + |\delta_{g-}|)/2$, and $\delta_v \equiv (|\delta_{v+}| + |\delta_{v-}|)/2$.

1) of A-type stars (cf. figure 4), which means that n_0^{III} (dominant stage) is not much sensitive to T .

Accordingly, the number populations of the lower level for the Ca I 6162 and Ca II 3934 lines ($n_{\text{low},61}$, $n_{\text{low},39}$) have the T -dependence of

$$n_{\text{low},61} \propto \exp[(6.11 + 11.87 - 1.90)/(kT)] \quad (5)$$

and

$$n_{\text{low},39} \propto \exp[(11.87 - 0.00)/(kT)], \quad (6)$$

where $\chi_{\text{low},61}^{\text{I}} = 1.90$ eV (for Ca I 6162), $\chi_{\text{low},39}^{\text{II}} = 0.00$ eV (for Ca II 3934), $\chi_{\text{ION}}^{\text{I}} = 6.11$ eV, and $\chi_{\text{ION}}^{\text{II}} = 11.87$ eV. Equations (5) and (6) explain the reason why W_{61} fades out more quickly (compared to W_{39}) with an increase in T_{eff} .

Since the abscissa of curve of growth is written as $A + \log n_{\text{low}} + \log gf$ (+const.), empirical curves of growth in the present cases of two lines can be constructed based on the W and A results for 122 stars given in table 1 by plotting the $\log W_{61}$ vs. $A_{61} + \log n_{\text{low},61}$ (for Ca I 6162) and $\log W_{39}$ vs. $A_{39} + \log n_{\text{low},39}$ (for Ca II 3934) relations

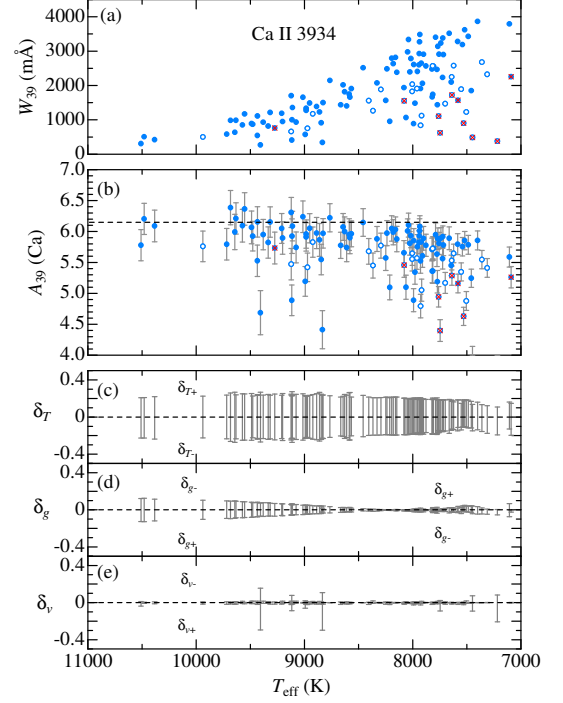


Fig. 3. Abundance-related results derived from 3910–3955 Å fitting (comprising Ca II 3934) plotted against T_{eff} . (a) Equivalent width of Ca II 3934 line (W_{39}), (b) $A_{39}(\text{Ca})$ (Ca abundance). Panels (c), (d), and (e) show the abundance perturbations in response to changing T_{eff} , $\log g$, and v_t evaluated in the same manner as in figure 2. Regarding the symbols in panels (a) and (b), Am stars are distinguished by open symbols as in figure 2, while overplotted red crosses indicate “broad weak K line” stars (labeled as BWK in the remark of table 1).

as shown in figures 5a and 5b, respectively, where T_{eff} has been assigned to T . It can be seen from figure 5 that Ca I 6162 line is on the linear ($W \propto A$) through flat part of the curve of growth, while Ca II 3934 line is mostly on the damping part of the curve of growth showing the square-root dependence of W upon A (except for several lines showing anomalous weakness).

5.2. Abundance sensitivity to atmospheric parameters

Some comments may be appropriate on the abundance sensitivities due to uncertainties of atmospheric parameters (cf. panels (c)–(e) in figures 2 and 3) based on what has been described in subsection 5.1.

As seen from these figure panels, Ca abundances are most sensitive to a change in T_{eff} (especially for early A stars). The strong T_{eff} -sensitivity can be explained by equations (5) and (6), which suggest $|\Delta A_{61}| \sim 16.08 \times (5040/T_{\text{eff}}^2) |\Delta T_{\text{eff}}|$ and $|\Delta A_{39}| \sim 11.87 \times (5040/T_{\text{eff}}^2) |\Delta T_{\text{eff}}|$. Inserting $T_{\text{eff}} = 8000$ K and $\Delta T_{\text{eff}} = 300$ K, for example, we have $|\Delta A_{61}| \sim 0.4$ dex and $|\Delta A_{39}| \sim 0.3$ dex, consistently with figures 2c and 3c.

In contrast, Ca abundances are not so sensitive to a change of $\log g$ (cf. figures 2d and 3d), especially for the damping-dominated strong Ca II 3934 line, because two effects caused by an increase $\log g$ compensate with each

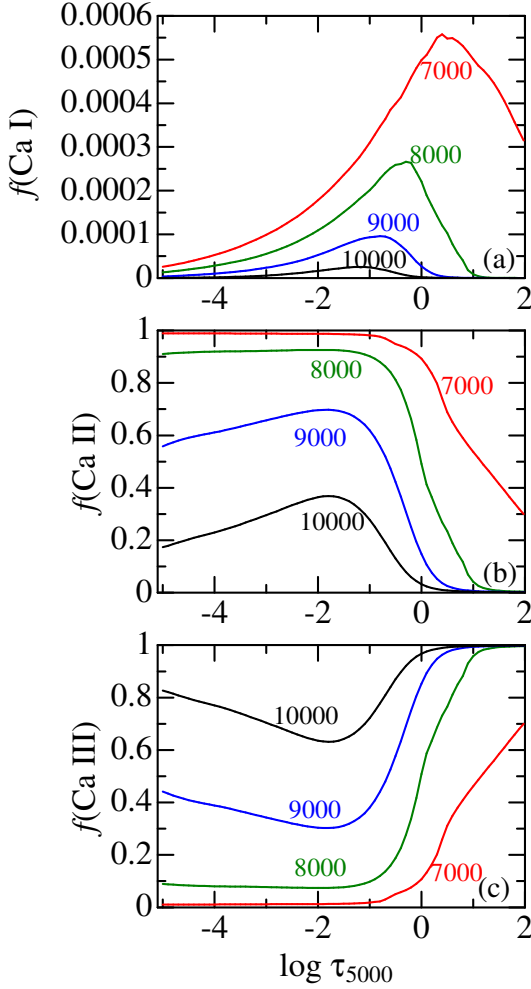


Fig. 4. Number population fraction (f) of (a) neutral, (b) once-ionized, and (c) twice-ionized calcium species relative to the total Ca atoms [e.g., $f(\text{Ca I}) \equiv N(\text{Ca I})/N_{\text{total}}^{\text{Ca}}$], plotted against the continuum optical depth at 5000 Å. Calculations were done for four $\log g = 4.0$ model of different T_{eff} (7000, 8000, 9000, and 10000 K) as indicated in each panel.

other: i.e., (i) enhanced continuum opacity (line weakening) and (ii) growth of damping wing (line strengthening).

Regarding the effect of changing v_t on the resulting abundances, the situation is markedly different between both lines (cf. figures 2e and 3e). Since the strength of Ca I 6162 (W_{61}) widely varies from very weak (linear part) at higher T_{eff} to strongly saturated (flat part) at lower T_{eff} , A_{61} is almost v_t -independent for early-A stars, while it is very sensitive to a choice of v_t for late-A stars ($T_{\text{eff}} \lesssim 8000$ K). In contrast, the role of v_t in determining A_{39} is essentially insignificant, because Ca II 3934 line is too strong (damping part) to be affected by v_t , though some exceptional v_t -sensitive cases exist where W_{39} is as low as several hundred mÅ.

5.3. Stars with anomalous Ca II 3934 line profile

Unexpectedly, embarrassing results were noticed from the 3910–3955 Å region fitting analysis (cf. section 4).

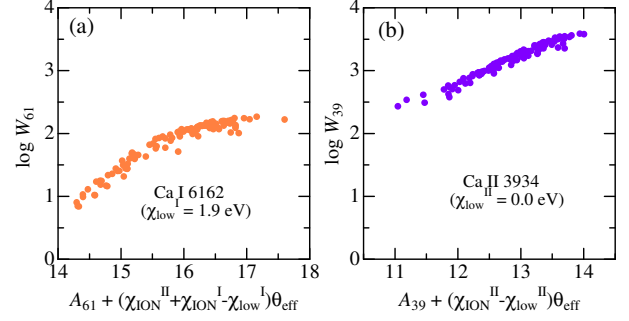


Fig. 5. Curves of growth for the Ca I 6162 and Ca II 3934 lines constructed from the equivalent widths (W) and the corresponding abundances (A) given in table 1. In panel (a) are plotted the $\log W_{61}$ values against $A_{61} + (\chi_{\text{ION}}^{\text{II}} + \chi_{\text{ION}}^{\text{I}} - \chi_{\text{low},61}^{\text{I}})\theta_{\text{eff}}$. Here, $\chi_{\text{ION}}^{\text{II}}$ ($= 11.87$ eV) and $\chi_{\text{ION}}^{\text{I}}$ ($= 6.11$ eV) are the ionization potentials of Ca II and Ca I, respectively, and $\chi_{\text{low},61}^{\text{I}}$ ($= 1.9$ eV) is the lower excitation potential of Ca I 6162, and $\theta_{\text{eff}} \equiv 5040/T_{\text{eff}}$. Similarly, panel (b) shows the relations between $\log W_{39}$ and $A_{39} + (\chi_{\text{ION}}^{\text{II}} - \chi_{\text{low},39}^{\text{II}})\theta_{\text{eff}}$, where $\chi_{\text{low},39}^{\text{II}}$ ($= 0.0$ eV) is the lower excitation potential of Ca II 3934.

That is, $v \sin i_{39}$ values for some of the program stars were found to be considerably discrepant from the $v \sin i_{61}$ solutions (regarded as standard $v \sin i$) derived from the 6140–6170 Å region fitting in Paper I, despite that both are based on the same spectra. These two $v \sin i$ values are compared in figures 6a and 6b, which elucidate that, in an appreciable fraction of slow rotators ($v \sin i_{61} \lesssim 100$ km s $^{-1}$), $v \sin i_{39}$ is considerably larger than $v \sin i_{61}$ even by up to ~ 200 –300% in extreme cases. It is on the side of $v \sin i_{39}$ (not $v \sin i_{61}$) that must be wrong in this context, because $v \sin i_{61}$ and $v \sin i_{58}$ (determined in Paper I from the spectrum fitting in the 5880–5905 Å region comprising Na I 5890/5896 lines) are still consistent with each other as shown in figures 6c and 6d.

A close inspection of these outliers revealed that the cause of this discrepancy stems from the anomalous profile of the Ca II 3934 line; i.e., it is unusually broad for its weak strength. The automatic fitting algorithm adopted in this study accomplishes the best parameter solutions that minimize the difference (χ^2) between the theoretical and observed spectra in the relevant wavelength region. As the Ca II K line is the dominant spectral feature in 3910–3955 Å, this program tries to adjust $v \sin i$ so as to fit this broad Ca II 3934 line, which eventually resulted in an spuriously large $v \sin i_{39}$. This is reason why an appreciable inequality ($v \sin i_{39} > v \sin i_{61}$) is seen in these stars.

Since such obtained $v \sin i_{39}$ solution is an appreciable overestimation for the actual projected rotational velocity, metallic line features other than Ca II 3934 can not be reproduced any more, which results in considerably poor fit for such lines (e.g., Fe I lines); see, e.g., the spectrum fit appearance in figure 1 for those peculiar objects such as HD 29499 (#90), HD 33204 (#107), HD 27628 (#111), and HD 33254 (#118). On the other hand, if the true $v \sin i$ is used as fixed, Ca II K line profile can never be

fitted no matter how $A_{39}(\text{Ca})$ is varied. This situation is demonstrated in figure 7, where the observed spectrum of HD 29499 (the star showing the largest anomaly of $v \sin i_{39}/v \sin i_{61} = 3.4$) is compared with theoretical spectra computed for 4 different Ca abundances but broadened with $v \sin i_{61} = 61 \text{ km s}^{-1}$ (real rotational velocity which adequately reproduces the profiles of neighboring metallic lines). This figure clearly shows that the observed Ca II K line is too broad (as if it is a damping-dominated line) despite that its strength is only mild (like lines in the flat-part of curve of growth).

Hereinafter, 10 especially anomalous stars with the criterion of $v \sin i_{39}/v \sin i_{61} (\equiv \alpha) > 1.5$ (i.e., discrepancy greater than 50%) are called “Weak Broad K-line stars” (abbreviated as WBK stars), which are marked by overplotted red crosses in figures 3a,b and figures 6a,b. They are also remarked in column 16 of table 1 and their HD numbers inserted in figure 1 are colored in red. The characteristics of these WBK stars can be summarized as follows.

- They are mostly late A-type stars at $T_{\text{eff}} \lesssim 8000 \text{ K}$ and show considerably low A_{39} and small W_{39} compared to other stars at the same T_{eff} (cf. figures 3a,b).
- They are slow rotators of $v \sin i_{61} \lesssim 100 \text{ km s}^{-1}$ (cf. figures 6a,b).
- As can be expected from the two characteristics mentioned above, most of them are classified as Am, though this does not mean that Am stars and WBK stars are equivalent (Am stars which do not show WBK phenomenon do exist).
- Since any satisfactory match could not be accomplished between the theoretical and observed spectrum in the 3910–3955 Å fitting, the resulting A_{39} (or $[\text{Ca}/\text{H}]_{39}$) and W_{39} for these stars (shown with parentheses in table 1) are unreliable³ and thus should be regarded with caution.
- It is difficult to understand the physical mechanism causing such an extraordinary WBK phenomenon, which is apparently inexplicable within the framework of the classical line-formation theory. A possibility of Ca abundance stratification was examined (cf. appendix 2), which however turned out unsuccessful.

5.4. Ca abundances from Ca I 6162 and Ca II 3934

We are now ready to address the questions raised in section 1: (i) How about the characteristics of the Ca abundances determined from Ca II K line (especially in relation to the Am phenomenon)? (ii) Are they consistent with those obtained from Ca I 6162 line? In figure 8 are plotted the resulting Ca abundances from both lines ($[\text{Ca}/\text{H}]_{39}$, $[\text{Ca}/\text{H}]_{61}$) along with their differences against T_{eff} and $v \sin i_{61}$.

³ Since a number of weaker metallic lines in the neighborhood of Ca II 3934 are regarded as if they are noises in such a case of unattained fit, A_{39} and W_{39} values tend to be underestimated, because the continuum level is wrongly placed too low.

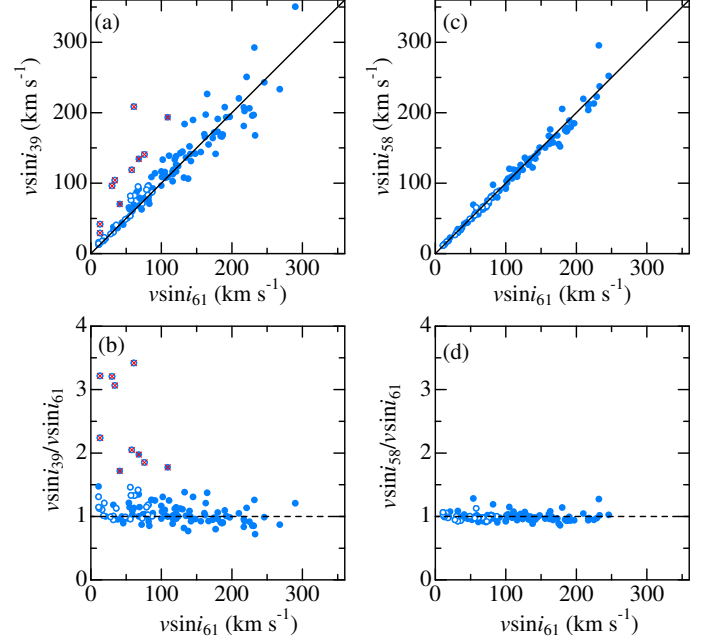


Fig. 6. Comparison of the standard $v \sin i$ values derived from 6140–6170 Å fitting in Paper I ($v \sin i_{61}$) with $v \sin i_{39}$ (from 3910–3955 Å fitting in this study) and $v \sin i_{58}$ (from 5880–5905 Å fitting in Paper I). (a) $v \sin i_{39}$ vs. $v \sin i_{61}$, (b) $v \sin i_{39}/v \sin i_{61}$ vs. $v \sin i_{61}$, (c) $v \sin i_{58}$ vs. $v \sin i_{61}$, and (d) $v \sin i_{58}/v \sin i_{61}$ vs. $v \sin i_{61}$. Am stars are distinguished by open symbols as in figures 2 and 3. As done in figures 3a and 3b, 10 weak broad K-line stars ($v \sin i_{39}/v \sin i_{61} > 1.5$) are marked by overplotted red crosses in the left-hand panels (a) and (b),

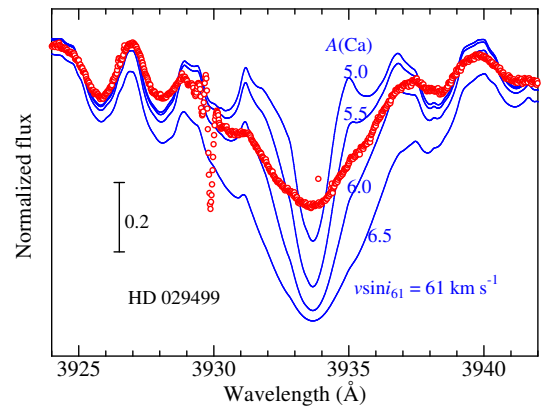


Fig. 7. Demonstration of how the typical “weak broad K line” star HD 29499 shows an anomalous Ca II 3934 line profile. Blue solid lines are theoretically synthesized profiles, which are computed for $A(\text{Ca}) = 5.0$ – 6.5 with a step of 0.5 dex and broadened with the standard $v \sin i_{61}$ of 61 km s^{-1} (actual projected rotational velocity for this star), while the observed profile is shown by red symbols (where the vertical offset and the global tilt are appropriately adjusted).

Let us discuss $[\text{Ca}/\text{H}]_{61}$ first. It can be seen from figure 8b that (i) the upper envelope of the distribution is $[\text{Ca}/\text{H}]_{61} \sim 0$ irrespective of T_{eff} , (ii) Am stars are generally underabundant in Ca compared to normal stars, and (iii) the extent of deficiency (lower envelope of the distribution) tends to increase with a decrease in T_{eff} . Furthermore, this deficiency of Ca has a systematic trend in terms of rotational velocity according to figure 8e, which shows that (iv) $[\text{Ca}/\text{H}]_{61}$ is nearly normal in rapid rotators ($v \sin i_{61} \gtrsim 100 \text{ km s}^{-1}$) while (v) begins to progressively decrease with a lowering of $v \sin i_{61}$ at $v \sin i_{61} \lesssim 100 \text{ km s}^{-1}$. These characteristics of $[\text{Ca}/\text{H}]_{61}$ seem to well fit the expectations from the diffusion theory, which predicts that photospheric Ca deficiency develops due to element segregation in the deeper stable radiative envelope of slow rotators (cf. the references quoted in section 1) and this anomaly tends to be enhanced towards lower T_{eff} (see, e.g., figure 14 in Richer et al. 2000).

In contrast, the behaviors of $[\text{Ca}/\text{H}]_{39}$ are rather different (although some similar tendency to that of $[\text{Ca}/\text{H}]_{61}$ is also seen in the qualitative sense): $[\text{Ca}/\text{H}]_{39}$ tends to be lower than $[\text{Ca}/\text{H}]_{61}$ and the difference tends to grow towards lower T_{eff} as displayed in figure 8c, which shows that $[\text{Ca}/\text{H}]_{39}$ is considerably below $[\text{Ca}/\text{H}]_{61}$ by ~ 1 dex or more in late A stars (especially Am stars) at $T_{\text{eff}} \lesssim 8000 \text{ K}$ while $[\text{Ca}/\text{H}]_{39}$ is nearly on the same order of (or slightly below) $[\text{Ca}/\text{H}]_{61}$ at early A stars ($T_{\text{eff}} \lesssim 8000 \text{ K}$). As a result, $[\text{Ca}/\text{H}]_{39}$ progressively declines with a decrease of T_{eff} for both Am and normal stars (cf. figure 8a). Meanwhile, this discrepancy seems to be independent of $v \sin i_{61}$ (figure 8f).

Also, with a suspicion that this T_{eff} -dependent Ca II–Ca I abundance difference might be due to a non-LTE effect, test non-LTE calculations were carried out for representative cases of different (T_{eff} , $A(\text{Ca})$) combinations. However, the resulting non-LTE corrections turned out to be too small to explain the problem. These supplementary calculations are separately described in appendix 1.

Accordingly, the following speculations may as well be made based on what has been elucidated regarding the characteristics of $[\text{Ca}/\text{H}]_{61}$ and $[\text{Ca}/\text{H}]_{39}$.

- Ca abundances derived from Ca I 6162 are considered to be reliable and thus $[\text{Ca}/\text{H}]_{61}$ represents the true photospheric abundance of calcium. Therefore, the observed characteristics of $[\text{Ca}/\text{H}]_{61}$ (see (i)–(v) above) may suggest that Ca is actually deficient in the atmosphere of Am stars, which stems from the atomic diffusion process operating in the stable radiative envelope of slow rotators.
- On the other hand, Ca abundances derived from Ca II 3934 are probably not correct especially for late A-type stars ($T_{\text{eff}} \lesssim 8000 \text{ K}$) where $[\text{Ca}/\text{H}]_{39}$ seems to be considerably underestimated in comparison with (presumably correct) $[\text{Ca}/\text{H}]_{61}$ by up to ~ 1 dex or more.
- However, the cause for this erroneous underestimation of $[\text{Ca}/\text{H}]_{39}$ is totally unknown. It may be possible that this has something to do with the

WBK phenomenon (cf. subsection 5.3), which is seen mainly in slowly rotating late A-type stars apparently showing conspicuously low $[\text{Ca}/\text{H}]_{39}$. Clarifying the reason why Ca II K line shows such an unusual behavior in slow rotators of cool A stars ($T_{\text{eff}} \lesssim 8000 \text{ K}$) should be an important issue to be addressed.

- As to the question regarding the cause for the weakness of Ca II K line in Am stars, which motivated this study, two compound factors seem to be responsible: (1) Deficiency of Ca abundance in the photosphere possibly resulting from the diffusion process (as indicated by $[\text{Ca}/\text{H}]_{61}$) is naturally the one reason. (2) Yet, there is more than that. Some unknown special mechanism of weakening Ca II 3934 line so operates in late A stars ($T_{\text{eff}} \lesssim 8000 \text{ K}$) as to further decrease the strength of this line. This synergy effect would be the reason why classical Am stars (mostly late A-type) show markedly weak Ca II K line.
- Accordingly, we would have to realize that some unknown aspect beyond our current comprehension (i.e., WBK phenomenon or extra weakening mechanism of Ca II K line) still exists regarding chemically peculiar stars (including Am stars) of upper main sequence. In this field of stellar physics, abundance anomaly caused by atomic diffusion has been the main stream interpretation for their spectrum peculiarity for almost a half century. Admittedly, this line of theoretical investigation is surely important and still to be pursued. In addition, however, it may be worth paying attention also to a possibility of non-classical atmospheric effect (e.g., stratification/ionization difference in slowly rotating stars compared to rapid rotators) such as previously considered by Böhm-Vitense (1976, 2006) for the cause of Am phenomenon.

5.5. Comparison with previous work

Finally, it may be worth comparing our W_{39} and A_{39} results with the data derived by Guthrie (1987), who determined the equivalent widths of Ca II K line and the resulting Ca abundances for a large number of 57 Am stars, though his work is based essentially on the literature data of k and $\text{Sp}(K)$ which were converted to W_{39} by using the empirical relation.

Since 13 Am stars of $T_{\text{eff}} \lesssim 8000 \text{ K}$ (#65, #75, #77, #86, #94, #95, #106, #107, #109, #111, #112, #118, and #119) among his 57 sample stars are in common with our program stars, comparisons of Ca II K-related results for these 13 objects are shown in figure 9. As can be seen from this figure, a considerably large discrepancy is seen in the sense that Guthrie's (1987) W_{39} as well as A_{39} are systematically large (by a factor of $\lesssim 2$ for W_{39} and by $\lesssim 1$ dex for A_{39} , even if excluding the data for WBK stars which are unreliable and probably underestimated; cf. footnote 3).

The author has no idea about the reason for such a se-

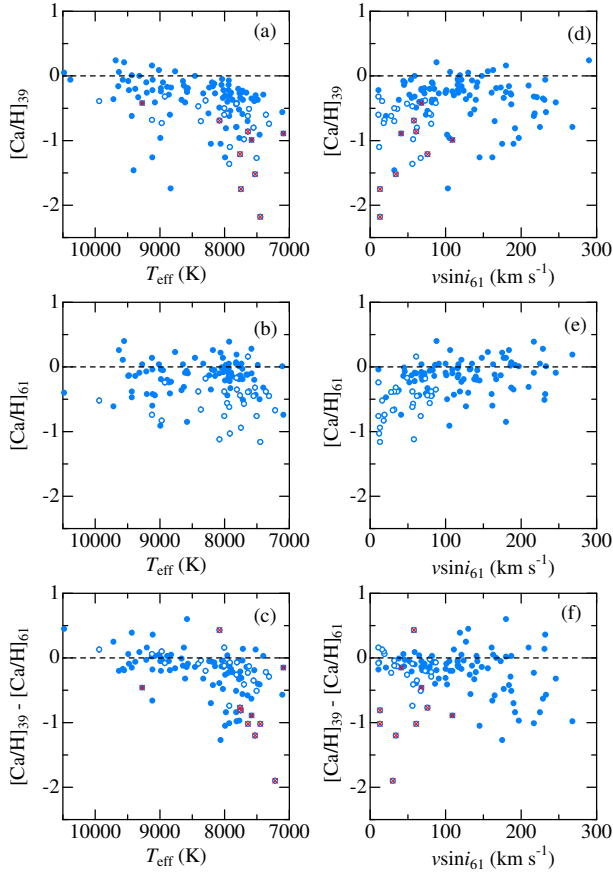


Fig. 8. Comparison of two Ca abundances (relative to the reference star Procyon; cf. table 1) corresponding to Ca II 3934 and Ca I 6162 lines and their trends in terms of T_{eff} and $v \sin i_{61}$. $[\text{Ca}/\text{H}]_{39}$, $[\text{Ca}/\text{H}]_{61}$, and $[\text{Ca}/\text{H}]_{39} - [\text{Ca}/\text{H}]_{61}$ are plotted against T_{eff} in the left-hand panels (a–c), and against $v \sin i_{61}$ in the right-hand panels (d–f). The meanings of the symbols are the same as in figure 7.

riously large difference. Since Guthrie’s analysis is based on the published literature data of photometric k index or K-line spectral type, its quantitative credibility may not be so high, especially for cool Am stars where contamination of neighboring metallic lines are significant. On the other hand, North et al. (1997) stated that their Ca II K line results for 23 Am stars based on spectrum synthesis (probably more reliable) are in good agreement with those of Guthrie (1987), though unfortunately North et al. did not publish any detailed data necessary for further check. If the conclusions of these previous investigations are correct, something might be wrong with the results of this study.

In any event, the problem is that research work on the Ca II K line in A-type stars has been insufficient so far as mentioned in section 1. Consequently, further follow-up study on this subject is necessary, by which more light would be shed on this situation.

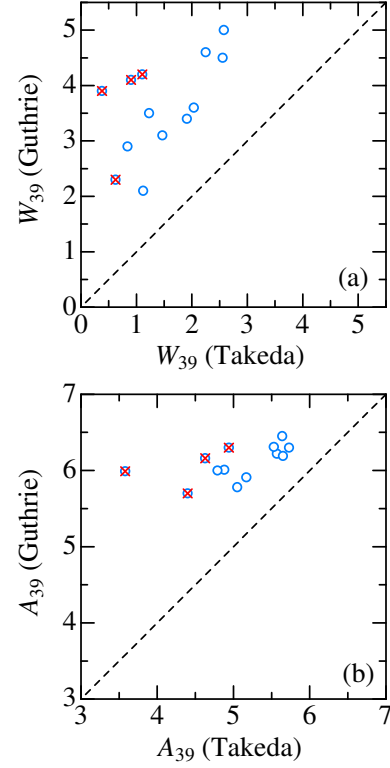


Fig. 9. Comparison of (a) W_{39} (equivalent width of Ca II 3934 in Å) and (b) A_{39} (logarithmic Ca abundance) derived by Guthrie (1987) based on Henry’s (1969) narrow-band K-line photometry data with those derived in this study, for 13 stars in common (all are cool Am stars of $T_{\text{eff}} \lesssim 8000$ K, among which 4 are weak broad K line stars). The same meanings of symbols as in figure 3.

6. Summary and conclusion

Despite that the strong Ca II K line at 3934 Å plays an important role in the spectral classification of upper main-sequence stars (its weakness is one of the criteria for Am stars), quantitative spectroscopic studies of this Ca II 3934 line for a large number of A-type stars have been insufficient so far, and the cause of Ca II K line weakening in relation to the Am phenomenon is not clarified yet. In order to address this issue, studying this Ca II K line along with the neutral Ca I lines for comparison should be worthwhile.

About a decade ago, Takeda et al. (2009) carried out a synthetic spectrum-fitting analysis applied to the 6140–6170 Å region for a large sample of 122 A-type main-sequence stars ($T_{\text{eff}} \sim 7000$ – 10000 K) in a wide range of rotational velocity ($v \sin i \sim 10$ – 300 km s^{-1}). Since this region included Ca I lines, Ca abundances from Ca I lines ($[\text{Ca}/\text{H}]_{61}$) and Ca I 6162 line strengths (W_{61}) are already available for these sample stars.

In this investigation, the same spectrum synthesis technique was applied anew to the 3910–3955 Å region (comprising Ca II 3934) to determine the Ca abundances from Ca II 3934 ($[\text{Ca}/\text{H}]_{39}$) and its line strengths (W_{39}) for these 122 program stars (including 28 Am stars) by using the same

observational data, in order to clarify (i) how the resulting Ca abundances are related with the Am phenomenon and (ii) whether $[\text{Ca}/\text{H}]_{39}$ and $[\text{Ca}/\text{H}]_{61}$ are consistent with each other.

It was confirmed that, for both Ca I and Ca II lines, Ca line strengths in Am stars tend to be weaker and associated abundances are lower compared to non-Am stars at the same T_{eff} , indicating a deficiency of Ca in the photosphere of Am stars which are mostly slow rotators. Since the upper envelope of $[\text{Ca}/\text{H}]_{61}$ vs. T_{eff} distribution is $[\text{Ca}/\text{H}]_{61} \sim 0$ (irrespective of T_{eff}) for normal A stars, it may be reasonable to state that Ca I 6162 line yields correct Ca abundances.

Regarding the comparison between $[\text{Ca}/\text{H}]_{39}$ and $[\text{Ca}/\text{H}]_{61}$, while both are roughly consistent with each other for hotter stars ($T_{\text{eff}} \gtrsim 8000$ K), the former tends to be lower (by up to ~ 1 dex or even more) than the latter for cooler A stars ($T_{\text{eff}} \lesssim 8000$ K). Accordingly, $[\text{Ca}/\text{H}]_{39}$ is likely to be erroneously underestimated in such late A-type stars for some unknown reason.

In addition, an appreciable fraction of these cool A (mostly Am) stars were found to show unusually anomalous Ca II 3934 line feature (i.e., extraordinarily broad for its considerable weakness) which is hard to explain. These “Weak Broad K-line” stars yielded apparently low Ca II K line strengths and $[\text{Ca}/\text{H}]_{39}$ values; but they are subject to large uncertainties (presumably underestimated) and thus unreliable, because theoretically synthesized spectrum could not fit the observed spectrum.

Accordingly, some special mechanism reducing the strength (and broaden the width) of Ca II 3934 line seems to be involved at $T_{\text{eff}} \lesssim 8000$ K where $[\text{Ca}/\text{H}]_{39}$ would be no more reliable.

Atomic diffusion process (causing the deficit of Ca in the photosphere as a result of element segregation in the deeper radiative envelope) is currently the promising explanation for the Am phenomenon, which seems to be consistent with the qualitative trend of $[\text{Ca}/\text{H}]_{61}$ in A-type stars. When it come to Ca II 3934 K line, however, its considerable weakness in classical Am stars should not necessarily be attributed to only this element diffusion scenario; i.e., some independent mechanism weakening this resonance line (specific to slowly rotating Am stars) may also be working.

As a last remark, the equivalent widths of the Ca II 3934 line measured in this study for cool Am stars (and the associated Ca abundances) appear to be in conflict (i.e., tend to be systematically smaller) with those of previous investigations. Further follow-up verification studies are to be desirably awaited.

This research has made use of the SIMBAD database, operated by CDS, Strasbourg, France. This investigation has also made use of the VALD database, operated at Uppsala University, the Institute of Astronomy RAS in Moscow, and the University of Vienna. Part of the observational data of this work is taken from the stellar spectra archive of the UVES Paranal Observatory Project (ESO DDT Program ID 266.D-5655).

Appendix 1. Non-LTE effect on Ca abundance determinations

Although a number of papers have been published on the non-LTE line formation of Ca II resonance lines at 3934 Å (K) and 3968 Å (H) for solar-type (F-, G-, and K-type) stars because core emission feature of these doublet lines is a good indicator of chromospheric activity, non-LTE effect on Ca abundance determinations in A-type stars (especially in relation to the Ca II K line) has been scarcely studied so far. As far as the author knows, it is probably only the following two investigations that are available at present: (i) Snijders (1975) carried out non-LTE calculations for Ca II in the T_{eff} range of 10000–15000 K (hot A and late B stars). His results are described in Leckrone (1976), who stated that the non-LTE effect depends on the treatment of UV flux. (ii) Stürenburg (1993) determined the non-LTE corrections for Ca I and Ca II lines for A-type stars of $T_{\text{eff}} \sim 7500$ –9000 K in his abundance analysis of λ Bootis stars. His results indicated that the non-LTE correction is line-dependent but quantitatively insignificant because its signs are negative and positive around zero.

On this occasion, the author conducted test non-LTE calculations for Ca I 6162 and Ca II 3934 lines in scope of A-type main-sequence stars, in order to examine whether or not the results of this study are significantly affected by the non-LTE effect. The atomic model and the computational procedure are the same as adopted by Takeda et al. (2010; cf. appendix B therein) in their non-LTE simulation of solar Ca II K line core emission profiles. The statistical-equilibrium calculations were carried out for three models with $T_{\text{eff}} = 7000, 8500, \text{ and } 10000$ K (each with the same solar-metallicity and $\log g = 4$) and $v_t = 2 \text{ km s}^{-1}$.

In figure 10 are shown the $l_0^{\text{NLTE}}(\tau)/l_0^{\text{LTE}}(\tau)$ (the NLTE-to-LTE line-center opacity ratio; nearly equal to $\simeq b_l$) and $S_L(\tau)/B(\tau)$ (the ratio of the line source function to the Planck function; nearly equal to $\simeq b_u/b_l$), where b_l and b_u are the non-LTE departure coefficients for the lower and upper levels, respectively) for each of the the Ca I 4^3P° – 5^3S transition (relevant to Ca I 6162 of multiplet 3) and Ca II 4^2S – 4^2P° transition (corresponding to Ca II 3934 of multiplet 1). Also, the LTE and non-LTE equivalent widths for the Ca I 6162 and Ca II 3934 lines along with the corresponding non-LTE abundance corrections were computed for each case, which are summarized in table 3.

An inspection of figure 10 and table 3 reveals the following characteristics regarding the non-LTE effect for these two Ca lines.

- Generally speaking, non-LTE departure is restricted to high atmosphere, and the non-LTE corrections (Δ) are insignificant for both lines ($\lesssim 0.1$ dex in most cases).
- Regarding Ca II 3934, Δ_{39} values are negative (corresponding to non-LTE line strengthening reflecting $S_L/B < 1$) but their extents are almost negligible, except for the saturated line case of high forming

depth ($W_{39} \lesssim 200$ mÅ for the t100g40 model with $A = 4.36$ in table 3) corresponding to the flat part of the curve of growth.

- In contrast, behaviors of Δ_{61} for Ca I 6162 are more complex, in the sense that its sign can be positive as well as negative. This is due to the fact that both opposite effects of (1) underpopulation of the lower level (line weakening) and (2) dilution of S_L (line strengthening) act in the formation of this line. Again, Δ_{61} becomes non-negligible for the cases of saturated lines ($W_{61} \sim 100$ – 200 mÅ; $A = 6.36$ case for t070g40 and t085g40 models).
- In any event, non-LTE effect is not quantitatively significant as far as the Ca lines used in this investigation for the analysis of A-type stars are concerned, which means that the assumption of LTE is reasonable in the practical sense. Also, the resulting trend of Δ values in table 3 indicates that these (conventionally evaluated) non-LTE corrections are unable to explain the serious discrepancy between $[\text{Ca}/\text{H}]_{39}$ and $[\text{Ca}/\text{H}]_{61}$ mentioned in subsection 5.4.

Appendix 2. Effect of abundance stratification on the Ca II K line profile

As described in subsection 5.3, the existence of ‘Weak Broad K line’ (WBK) stars, which are mainly seen in slowly rotating cool Am stars, was an embarrassing finding. How could such an extraordinary profile be possible?

When it comes to anomalous Ca II 3934 line profile in chemically peculiar stars, what comes to our mind is the case of some cool Ap stars showing a peculiar K line profile with sharp core and broad wing. This unusual Ca II K line shape is nowadays considered to be due to the stratified Ca abundance in the atmosphere (i.e., Ca atoms settle out towards deeper subphotospheric layer, leading to a deficiency in the upper atmosphere and an overabundance in the deep photosphere). Actually, an appropriately adjusted stratified model of Ca distribution can reproduce the observed K line profile of such Ap stars remarkably well (see, e.g., figure 3 in Ryabchikova 2014).

This is demonstrated in figure 11, where two Ca II K lines profiles computed for two cases of Ca distribution (homogeneous case and stratified case) are compared with each other. Here, the atmospheric parameters and the Ca abundance profile were chosen by consulting figure 4 of Ryabchikova (2014). It can be seen from this figure that the stratification of Ca atoms can produce such a characteristic profile (with wider wing and sharper core in comparison with normal profile) as actually observed in Ap stars (e.g., 10 Aql).

However, these examples in figure 11 correspond to the case of damping-dominated strong line and do not represent the weak Ca II K line as observed in WBK stars ($W_{39} \lesssim 1000$ mÅ; cf. figure 3a). Therefore, simulations were carried out to examine whether it is possible to produce weak but broad profile by adequately adjusting the stratified Ca abundance distribution. The results are de-

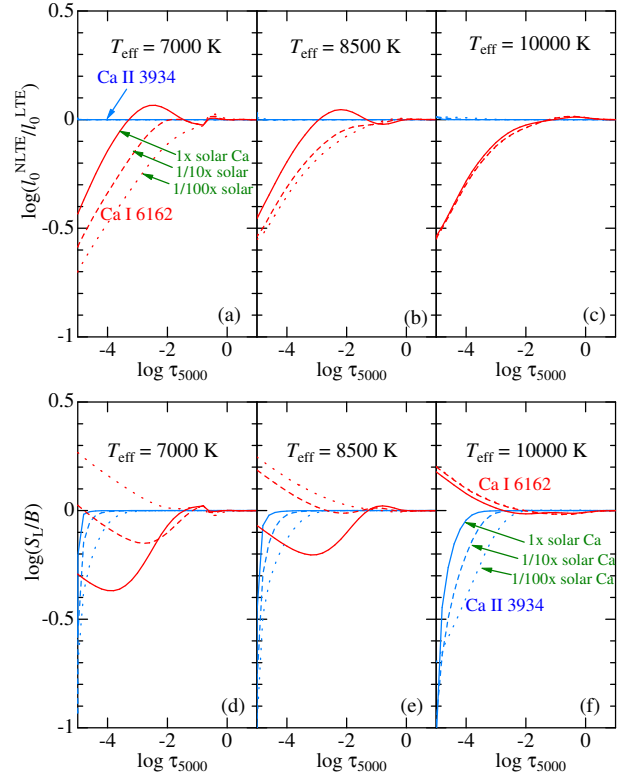


Fig. 10. The NLTE-to-LTE line-center opacity ratio (upper panels a–c) and the ratio of the line source function (S_L) to the local Planck function (B) (lower panels d–f) for the Ca I 4^3P^o – 5^3S transition of Ca I 6162 (red lines) and the Ca II 4^2S – 4^2P^o transition of Ca II 3934 (blue lines), plotted against the continuum optical depth at 5000 Å. Computations were done on three $\log g = 4.0$ solar-metallicity models with different T_{eff} of 7000 K (left panels a, d), 8500 K (middle panels b, e), and 10000 K (right panels c, f), for three Ca abundances of $A(\text{Ca}) = 6.36$ (solar), 5.36 ($1/10 \times$ solar) and 4.36 ($1/100 \times$ solar) as depicted in solid, dashed, and dotted lines, respectively.

picted in figure 12 (see the caption of this figure for the details of this test calculation). Although we refrain from going into in-depth discussion, one important conclusion elucidated from figure 12 should be mentioned: In case where the line strength is considerably weak ($\log W \lesssim 3$) compared to those of normal A stars, the line profile can not be made significantly different from that of the ordinary homogeneous case (cf. the left part of each panels b–d and f–h in figure 12, where we can see that symbols are asymptotically merged with the red line), no matter how the distribution of Ca stratification is changed (as far as the present modeling is concerned). Accordingly, it may be concluded that the depth-dependent Ca abundance distribution can not be an explanation for the WBK phenomenon.

References

- Bagnulo, S., Jehin, E., Ledoux, C., Cabanac, R., Melo, C., Gilmozzi, R., & the ESO Paranal Science Operations Team 2003, ESO Messenger, 114, 10

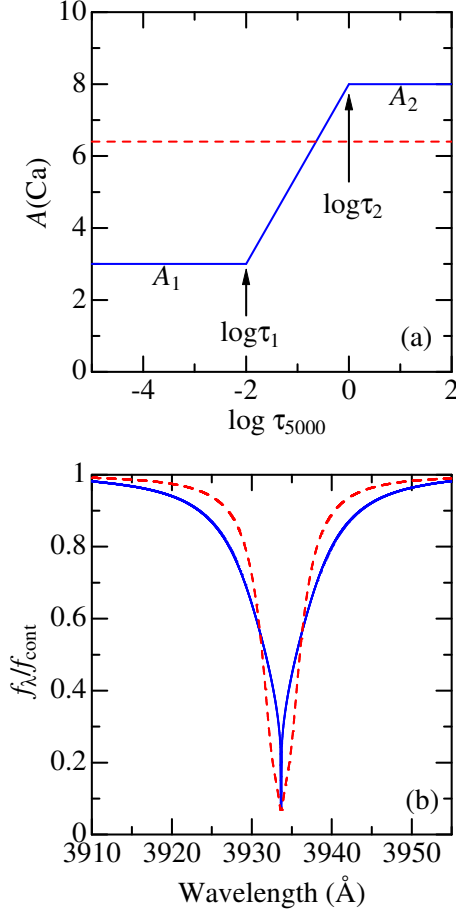


Fig. 11. Demonstrative Ca II 3934 profile simulation carried out on the representative $T_{\text{eff}} = 7500$ K and $\log g = 4.0$ model for two different Ca distributions as illustrated in panel (a): (i) depth-independent homogeneous Ca abundance of $A = 6.4$ (red dashed line) and (ii) stratified Ca abundances with $A_1 = 3.0$, $A_2 = 8.0$, $\log \tau_1 = -2$, and $\log \tau_2 = 0$ (blue solid line). The resulting profiles for the two cases are depicted in panel (b).

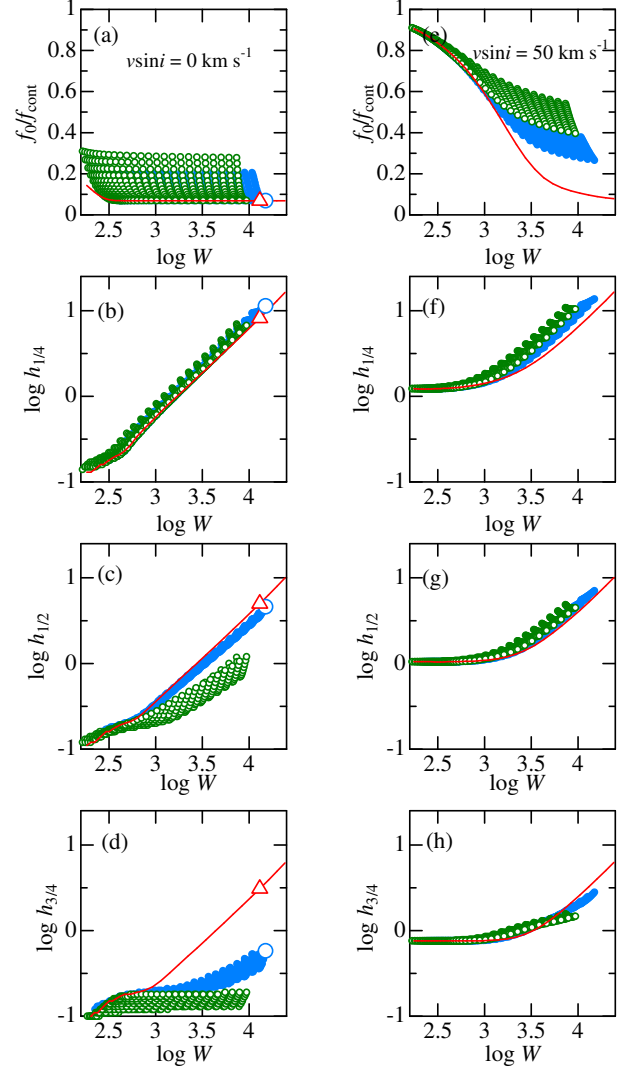


Fig. 12. Characteristics of theoretical Ca II 3934 line profiles simulated for many stratified Ca abundance distributions where the combinations of (A_1, A_2) are variously changed in the ranges of $A_1 = 0-3$ and $A_2 = 3-8$ (with a step of 0.2 dex), while two cases are assumed for the critical optical depths: (i) gradual gradient with $(\log \tau_1, \log \tau_2) = (-2, 0)$ and (ii) steeper gradient with $(\log \tau_1, \log \tau_2) = (-1, 0)$. In panels (a/e), (b/f), (c/g), and (d/h) are plotted the line-center residual flux (f_0/f_{cont}), 1/4-maximum width ($h_{1/4}$), half-maximum width ($h_{1/2}$), and 3/4-maximum width ($h_{3/4}$) against the correspondent equivalent width (W), where h is in unit of Å and W is in mÅ. The left-hand panels (a-d) and right-hand panels (e-h) correspond to the unbroadened profiles ($v \sin i = 0$ km s $^{-1}$) and rotationally broadened profiles with $v \sin i = 50$ km s $^{-1}$, respectively. Case (i) and case (ii) results are expressed in blue filled circles and green open circles, respectively. The results for the case of homogeneous Ca abundance ($A_1 = A_2$) are shown by red solid lines for comparison. Two large open symbols in the left-hand panels (a-d) correspond to two example cases shown in figure 11.

- Böhm-Vitense, E. 1976, in Physics of Ap Stars, Proc. IAU Colloq. 32, ed. W.W. Weiss, H. Jenkner, & H.J. Wood (Univ. Wien), 633
- Böhm-Vitense, E. 2006, PASP, 118, 419
- Conti, P. S. 1965, ApJS, 11, 47
- Conti, P. S. 1970, PASP, 82, 781
- Gebran, M., Vick, M., Monier, R., & Fossati, L. 2010, A&A, 523, A71
- Guthrie, B. N. G 1987, MNRAS, 226, 361
- Henry, R. C. 1969, ApJS, 18, 47
- Hoffleit, D., & Jaschek, C. 1982, The Bright Star Catalogue, Fourth Revised Edition (Yale University Observatory: New Haven, CT)
- Hui-Bon-Hoa, A. 2000, A&AS, 144, 203
- Kurucz, R. L. 1993, Kurucz CD-ROM, No. 13 (Harvard-Smithsonian Center for Astrophysics)
- Kurucz, R. L., & Bell, B. 1995, Kurucz CD-ROM, No. 23 (Harvard-Smithsonian Center for Astrophysics)
- Leckrone, D. S. 1976, in Physics of Ap Stars, Proc. IAU Colloq. 32, ed. W.W. Weiss, H. Jenkner, & H.J. Wood (Univ. Wien), 465

- Napiwotzki, R., Schönberner, D., & Wenske, V. 1993, *A&A*, 268, 653
- North, P., Jaschek, C., Hauck, B., Figueras, F., Torra, J., & Künzli, M. 1997, *ESASP*, 402, 239
- Richer, J., Michaud, G., & Turcotte, S. 2000, *ApJ*, 529, 338
- Ryabchikova, T. 2014, in *Determination of Atmospheric Parameters of B-, A-, F- and G-Type Stars (Lectures from the School of Spectroscopic Data Analyses)*, ed. E. Niemczura, B. Smalley, & W. Pych (Springer International Publishing: Switzerland)
- Ryabchikova, T., Piskunov, N., Kurucz, R. L., Stempels, H. C., Heiter, U., Pakhomov, Yu, & Barklem, P. S. 2015, *Phys. Scr.*, 90, 054005
- Smith, M. A. 1973, *ApJS*, 25, 277
- Snijders, M. A. J. 1975, *BAAS*, 7, 469
- Stürenburg, S. 1993, *A&A*, 277, 139
- Takeda, Y. 1995, *PASJ*, 47, 287
- Takeda, Y., Kang, D.-I., Han, I., Lee, B.-C., & Kim, K.-M. 2009, *PASJ*, 61, 1165 (Paper I)
- Takeda, Y., Han, I., Kang, D.-I., Lee, B.-C., & Kim, K.-M. 2008, *JKAS*, 41, 83
- Takeda, Y., Honda, S., Kawanomoto, S., Ando, H., & Sakurai, T. 2010, *A&A*, 515, A93
- Talon, S., Richard, O., & Michaud, G. 2006, *ApJ*, 645, 634
- Varenne, O., & Monier, R. 1999, *A&A*, 351, 247
- Watson, W. D. 1971, *A&A*, 13, 263

Table 1. Basic stellar data and the results of the analysis.

star#	HD#	HR#	Name	Sp.type	T_{eff}	$\log g$	v_t	$v \sin i_{61}$	[Fe/H] ₆₁	[Ca/H] ₆₁	W_{61}	[Ca/H] ₃₉	W_{39}	α	Remark
1	130109	5511	109 Vir	A0V	9683	3.68	2.4	290	-0.80	+0.24	985	1.21	
2	192696	7740	33 Cyg	A3IV-Vn	7815	3.49	4.0	268	-0.30	+0.19	164	-0.79	1741	0.87	
3	38678	1998	ζ Lep	A2Vann	8610	3.96	3.7	246	-0.48	-0.09	69	-0.41	1404	0.99	
4	28024	1392	ν Tau	A8Vn	7107	3.20	3.3	233	-0.05	+0.01	167	-0.56	3793	0.72	
5	19275	932		A2Vnn	9111	4.12	3.2	232	-0.16	-0.42	18	-0.06	1358	1.26	
6	187642	7557	α Aql	A7IV-V	7717	4.00	3.9	231	+0.19	-0.51	104	-0.37	2899	0.85	
7	203280	8162	α Cep	A7IV-V	7585	3.73	3.8	229	+0.14	+0.28	185	-0.36	3280	0.86	
8	92769	4189	40 LMi	A4Vn	7820	4.01	4.0	225	-0.06	+0.05	156	-0.79	1666	0.92	
9	14055	664	γ Tri	A1Vnn	9335	3.98	2.9	221	+0.00	-0.33	819	1.13	
10	118098	5107	ζ Vir	A3V	8249	4.02	4.0	218	+0.16	-0.58	1565	0.93	
11	33111	1666	β Eri	A3IIIvar	7928	3.59	4.0	217	+0.02	+0.39	175	-0.62	1910	0.83	
12	116842	5062	80 UMa	A5V SB	7942	4.02	4.0	217	-0.10	-0.09	134	-0.32	2600	0.96	
13	106591	4660	δ UMa	A3Vvar	8629	3.85	3.7	210	-0.38	-0.31	46	-0.15	1817	1.05	
14	19107	925	ρ^3 Eri	A8V	7772	3.96	4.0	197	+0.00	+0.01	155	-0.96	1438	0.99	
15	37507	1937	49 Ori	A4V	7979	3.82	4.0	192	-0.06	+0.03	140	-0.81	1484	1.01	
16	126248	5392		A5V	8212	4.02	4.0	190	-0.15	-0.35	83	-1.05	957	1.09	
17	79439	3662	18 UMa	A5V	7822	4.03	4.0	187	+0.08	+0.07	158	-0.44	2478	0.90	
18	27946	1388	κ^2 Tau	A7V	7401	3.84	3.7	187	-0.06	-0.32	136	-0.29	3865	0.90	
19	197950	7945	4 Cep	A8V	7768	4.08	4.0	186	+0.20	+0.02	157	-0.27	3139	0.89	
20	97603	4357	δ Leo	A4V	8180	3.90	4.0	184	+0.06	+0.26	148	-0.16	2636	0.91	
21	141003	5867	β Ser	A3V	8580	3.56	3.7	180	-0.47	-0.85	15	-0.25	1662	1.06	
22	16970	804	γ Cet	A3V	9122	4.05	3.2	180	+0.08	+0.14	45	+0.16	1704	0.96	
23	102124	4515	ξ Vir	A4V	8026	4.09	4.0	177	+0.24	+0.14	152	-0.34	2395	0.80	
24	18978	919	τ^3 Eri	A4V	8062	4.03	4.0	175	+0.09	+0.22	155	-1.05	1067	0.98	
25	59037	2857	γ^4 Gem	A4V	8238	3.99	4.0	173	-0.07	-0.13	105	-0.18	2484	0.95	
26	192425	7724	ρ Aql	A2V	8984	4.21	3.3	167	+0.18	-0.19	37	-0.19	1337	0.93	
27	30780	1547	97 Tau	A7IV-V	7644	3.87	3.9	165	-0.07	-0.12	147	-0.70	2100	1.37	
28	80081	3690	38 Lyn	A1V	9014	3.82	3.3	163	-0.36	+0.04	39	+0.09	1657	1.21	
29	110411	4828	ρ Vir	A0V	9117	4.22	3.2	162	-0.47	-0.61	13	-1.26	412	1.02	
30	103287	4554	γ UMa	A0V SB	9202	3.79	3.0	161	-0.21	-0.42	11	-0.26	950	1.05	
31	6695	328	ψ^2 Psc	A3V	8765	4.13	3.6	156	-0.12	+0.23	89	+0.07	2147	0.92	
32	56537	2763	λ Gem	A3V...	8458	3.90	3.8	148	-0.10	+0.14	106	+0.00	2516	0.96	
33	135559	5679	4 Ser	A4V	7992	4.14	4.0	145	-0.14	-0.21	119	-1.26	889	1.31	
34	20677	1002	32 Per	A3V	8952	4.08	3.3	142	+0.04	-0.05	46	-0.10	1490	0.92	
35	210418	8450	θ Peg	A2V	8888	3.82	3.4	141	-0.43	-0.20	33	-0.17	1388	1.00	
36	87696	3974	21 LMi	A7V	7878	4.13	4.0	140	-0.11	-0.15	133	-0.37	2569	1.09	
37	8538	403	δ Cas	A5Vv SB	7776	3.41	4.0	138	-0.16	-0.19	128	-0.52	2468	0.77	
38	76644	3569	ι UMa	A7IV	7934	4.22	4.0	135	-0.13	+0.05	151	-0.07	3485	1.01	
39	91312	4132		A7IV	7724	4.08	3.9	133	-0.10	-0.03	152	-0.59	2234	1.38	
40	29488	1479	σ^2 Tau	A5Vn	7990	3.82	4.0	132	-0.08	-0.04	132	-0.30	2610	0.82	
41	222661	8988	ω^2 Aqr	B9V	10481	4.28	1.5	130	-0.13	-0.40	1	+0.05	509	1.11	
42	71155	3314		A0V	9718	4.11	2.4	127	-0.39	-0.61	3	-0.36	584	1.12	
43	99211	4405	γ Crt	A9V	7722	3.95	3.9	124	-0.16	-0.19	137	-0.23	3383	1.00	
44	218045	8781	α Peg	B9.5III	9643	3.52	2.5	121	-0.34	-0.16	637	1.14	
45	1404	68	σ And	A2V	8828	4.00	3.5	121	-0.29	-0.23	40	-0.18	1501	0.96	
46	139006	5793	α CrB	A0V	9573	3.87	2.5	121	-0.16	+0.11	15	-0.06	852	1.04	
47	213558	8585	α Lac	A1V	9434	4.14	2.7	119	-0.21	-0.38	10	+0.01	1112	1.12	
48	127762	5435	γ Boo	A7IIIvar	7663	3.59	3.9	117	-0.23	-0.12	143	-0.26	3518	1.02	
49	102647	4534	β Leo	A3Vvar	8643	4.17	3.7	117	-0.07	+0.04	85	-0.08	2018	0.97	
50	28527	1427		A6IV	8039	3.99	4.0	116	+0.01	-0.01	134	-0.05	3338	0.88	
51	32301	1620	ι Tau	A7V	7937	3.74	4.0	116	-0.07	-0.02	136	-0.14	3271	0.97	
52	177196	7215	16 Lyr	A7V	7940	4.10	4.0	116	-0.09	-0.16	128	-0.22	2929	1.01	
53	28910	1444	ρ Tau	A8V	7520	3.97	3.8	111	-0.24	-0.43	124	-0.30	3621	1.25	
54	137898	5746	10 Ser	A8IV	7582	3.97	3.8	109	-0.05	-0.10	152	(-0.99)	(1569)	1.77	WBK
55	48097	2466	26 Gem	A2V	8984	4.23	3.3	109	-0.12	-0.04	48	-0.24	1275	1.00	
56	200761	8075	θ Cap	A1V	9633	4.11	2.5	106	+0.02	+0.26	23	+0.06	988	1.02	
57	31295	1570	π^1 Ori	A0V	8993	4.11	3.3	105	-0.72	-0.91	8	-0.96	576	1.10	
58	125162	5351	λ Boo	A0sh	8834	4.08	3.5	103	-1.54	-1.74	343	1.06	
59	85376	3900	22 Leo	A5IV	7459	3.98	3.7	102	-0.18	-0.50	117	-0.91	1851	1.31	
60	31647	1592	ω Aur	A1V	9478	4.27	2.7	101	+0.00	-0.13	17	-0.22	871	1.08	
61	6961	343	θ Cas	A7Vvar	7900	3.81	4.0	100	+0.07	-0.09	133	-0.26	2908	0.96	
62	18454	883	4 Eri	A5IV/V	7740	4.07	3.9	100	+0.21	+0.05	159	-0.26	3234	1.17	
63	76543	3561	σ^1 Cnc	A5III	8330	4.18	3.9	91	+0.31	+0.05	117	-0.27	2075	1.25	
64	12216	580	50 Cas	A2V	9553	3.90	2.6	88	+0.15	+0.40	28	+0.21	1172	1.05	
65	28355	1414	79 Tau	A7V	7809	3.98	4.0	87	+0.15	-0.35	115	-0.42	2557	1.00	Am
66	222345	8968	ω^1 Aqr	A7IV	7487	3.88	3.8	86	-0.07	+0.03	168	-0.37	3428	1.26	
67	74198	3449	γ Cnc	A1IV	9381	4.11	2.8	85	+0.26	-0.14	18	-0.20	931	1.01	
68	27934	1387	κ^1 Tau	A7IV-V	8159	3.84	4.0	83	+0.00	-0.05	116	-0.12	2817	0.85	
69	25490	1251	ν Tau	A1V	9077	3.93	3.2	82	+0.01	-0.44	15	-0.41	934	0.98	
70	29388	1473	90 Tau	A6V	8194	3.88	4.0	82	-0.03	-0.03	116	-0.10	2795	0.92	
71	79469	3665	θ Hya	B9.5V	10510	4.20	1.4	82	-0.01	-0.37	308	1.18	
72	28226	1403		Am	7361	4.01	3.6	81	+0.25	-0.38	128	-0.60	2681	1.02	Am
73	207098	8322	δ Cap	A5mF2 (IV)	7312	4.06	3.6	81	+0.10	-0.45	123	-0.74	2325	1.18	Am
74	216627	8709	δ Aqr	A3V	8587	3.59	3.7	79	-0.26	-0.06	63	-0.20	1750	1.02	
75	33641	1689	μ Aur	A4m	7961	4.21	4.0	79	+0.08	-0.56	85	-0.58	1910	1.15	Am
76	12111	575	48 Cas	A3IV	7910	4.08	4.0	76	-0.26	-0.33	112	-0.55	2062	1.04	
77	23281	1139		A5m	7761	4.19	4.0	76	+0.03	-0.44	112	(-1.21)	(1106)	1.85	Am, WBK
78	192640	7736	29 Cyg	A2V	8845	3.86	3.5	74	-1.54	-0.41	25	-0.60	915	1.03	
79	11636	553	β Ari	A5V...	8294	4.12	3.9	73	+0.10	-0.18	96	-0.38	1885	0.97	Am
80	173880	7069	111 Her	A5III	8567	4.27	3.8	72	+0.20	-0.10	82	-0.19	1908	1.01	
81	5448	269	μ And	A5V	8147	3.82	4.0	72	-0.14	-0.14	107	-0.27	2383	0.87	
82	17093	812	38 Ari	A7III-IV	7541	3.95	3.8	69	-0.25	-0.20	144	-0.39	3191	1.15	
83	28319	1412	θ^2 Tau	A7III	7789	3.68	4.0	68	-0.11	-0.15	134	-0.20	3403	1.35	
84	95382	4294	59 Leo	A5III	8017	3.95	4.0	68	-0.10	-0.08	128	-0.22	2785	1.00	
85	140436	5849	γ CrB	A1Vs	9274	3.89	3.0	68	-0.21	+0.05	25	(-0.42)	(762)	1.98	WBK
86	20320	984	ζ Eri	A5m	7505	3.91	3.8	67	-0.13	-0.76	90	-1.27	1228	1.42	Am
87	13161	622	β Tri	A5III	7957	3.68	4.0	65							

Table 1. (Continued.)

star#	HD#	HR#	Name	Sp.type	T_{eff}	$\log g$	v_t	$v \sin i_{61}$	[Fe/H] ₆₁	[Ca/H] ₆₁	W_{61}	[Ca/H] ₃₉	W_{39}	α	Remark
93	130841	5531	α^2 Lib	A3IV	8079	3.96	4.0	58	-0.37	-1.12	27	(-0.69)	(1554)	2.05	Am, WBK
94	30121	1511	4 Cam	A3m	7700	3.98	3.9	57	+0.25	-0.58	98	-0.98	1469	1.33	Am
95	30210	1519		Am...	7927	3.94	4.0	56	+0.44	-0.62	77	-1.36	840	1.46	Am
96	29479	1478	σ^1 Tau	A4m	8406	4.14	3.9	56	+0.35	-0.38	66	-0.47	1559	0.96	Am
97	222603	8984	λ Psc	A7V	7757	3.99	4.0	55	-0.19	-0.13	143	-0.34	2911	1.14	
98	212061	8518	γ Aqr	A0V	10384	3.95	1.5	54	-0.01	-0.06	422	1.21	
99	89021	4033	λ UMa	A2IV	8861	3.61	3.5	52	+0.06	-0.24	28	-0.29	1230	0.97	
100	195725	7850	θ Cep	A7III	7816	3.74	4.0	49	+0.14	-0.17	131	-0.43	2569	0.99	Am
101	43378	2238	2 Lyn	A2Vs	9210	4.09	3.0	46	-0.15	-0.07	28	-0.10	1191	0.89	
102	27819	1380	δ^2 Tau	A7V	8047	3.95	4.0	45	-0.04	-0.01	132	-0.14	2977	0.93	
103	95418	4295	β UMa	A1V	9489	3.85	2.7	44	+0.21	-0.14	10	-0.08	891	1.00	
104	218396	8799		A5V	7091	4.06	3.3	41	-0.58	-0.74	101	(-0.89)	(2255)	1.72	WBK
105	84107	3861	15 Leo	A2IV	8665	4.31	3.7	38	+0.01	-0.36	50	-0.37	1438	0.95	
106	204188	8210		A8m	7622	4.21	3.9	36	+0.02	-0.38	123	-0.51	2577	1.13	Am
107	33204	1670		A5m	7530	4.06	3.8	34	+0.28	-0.32	133	(-1.52)	(902)	3.06	Am, WBK
108	141795	5892	ϵ Ser	A2m	8367	4.24	3.9	32	+0.23	-0.66	46	-0.70	1264	1.01	Am
109	173648	7056	ζ^1 Lyr	Am	8004	3.90	4.0	32	+0.29	-0.38	96	-0.50	2036	0.95	Am
110	112185	4905	ϵ UMa	A0p	9407	3.61	2.8	32	+0.17	-1.46	271	1.18	
111	27628	1368	60 Tau	A3m	7218	4.05	3.5	30	+0.32	-0.67	104	(-2.57)	(379)	3.21	Am, WBK
112	28546	1428	81 Tau	Am	7640	4.17	3.9	28	+0.22	-0.39	122	-0.62	2249	0.99	Am
113	172167	7001	α Lyr	A0Vvar	9435	3.99	2.7	21	-0.55	-0.47	7	-0.62	546	1.00	
114	60179	2891	α Gem	A2Vm	9122	3.88	3.2	19	-0.03	-0.74	7	-0.68	660	1.21	Am
115	95608	4300	60 Leo	A1m	8972	4.20	3.3	18	+0.30	-0.83	11	-0.73	754	1.01	Am
116	48915	2491	α CMa	A0m...	9938	4.31	2.1	16	+0.42	-0.52	3	-0.39	502	1.11	Am
117	27749	1376	63 Tau	A1m	7448	4.21	3.7	13	+0.47	-1.16	51	(-2.18)	(487)	2.24	Am, WBK
118	33254	1672	16 Ori	A2m	7747	4.14	3.9	13	+0.38	-0.95	59	(-1.75)	(623)	3.22	Am, WBK
119	72037	3354	2 UMa	A2m	7918	4.16	4.0	12	+0.21	-1.03	43	-1.10	1121	1.12	Am
120	27962	1389	δ^3 Tau	A2IV	8923	3.94	3.4	11	+0.23	-0.24	31	-0.32	1174	1.15	Am
121	47105	2421	γ Gem	A0IV	9115	3.49	3.2	11	-0.06	-0.03	21	-0.22	1002	1.47	
122	40932	2124	μ Ori	Am...	8005	3.93	4.0	11	-0.12	-0.76	58	-0.60	1827	1.31	Am

In columns 1–8 are given the star number (arbitrarily assigned in this study), HD number, HR number, star name (with constellation), spectral type (taken from the Bright Star Catalogue; Hoffleit & Jaschek 1982), effective temperature (in K), logarithmic surface gravity (in $\text{cm s}^{-2}/\text{dex}$), and microturbulent velocity (in km s^{-1}), which are the same as in table 1 of Paper I. Columns 9 through 12 present the results (designated by suffix “61”) obtained from the 6140–6170 Å region fitting carried out in Paper I: the projected rotational velocity (in km s^{-1}), Fe abundance, Ca abundance and the equivalent width of Ca I 6162 line. The Ca abundance and equivalent width of the Ca II 3934 line (designated by suffix “39”) obtained from the 3910–3955 Å region fitting analysis of this study are given in columns 13 and 14, respectively. Column 15 presents $v \sin i_{39}/v \sin i_{61}$ ($\equiv \alpha$), which is the ratio of $v \sin i$ values derived from two fitting analyses of 3910–3955 Å region and 6140–6170 Å region. In the final column 16, “Am” means stars classified as metallic-line star in (at least one of) the published spectral classifications compiled in the SIMBAD database (note that this does not necessarily consistent with the spectral type given in column 5), and “WBK” denotes Weak Broad K-line star (defined by the criterion $\alpha > 1.5$). All the abundance results ($[X/H]$; in dex) are the differential values relative to Procyon ($A_{61}^{\text{Fe}} = 7.49$, $A_{61}^{\text{Ca}} = 6.19$, and $A_{39}^{\text{Ca}} = 6.15$, which are almost equivalent to the solar abundances) and equivalent widths are in mÅ. The parenthesized values in columns 13 and 14 are unreliable and thus should not be seriously taken because they are of the anomalous Weak Broad K-line stars. The 122 stars are arranged in the descending order of $v \sin i_{61}$, to make it consistent with figure 1 (and figure 2 in Paper I).

Table 2. Atomic data of Ca I 6162 and Ca II 3934 lines used in the spectrum synthesis.

RMT	λ (Å)	χ_{low} (eV)	$\log gf$ (dex)	Gammar (dex)	Gammas (dex)	Gammaw (dex)	Source
1	3933.655	0.000	-2.623	8.21	-5.73	-7.76	VALD
1	3933.657	0.000	-4.293	8.21	-5.73	-7.76	VALD
1	3933.659	0.000	-1.576	8.21	-5.73	-7.76	VALD
1	3933.660	0.000	-2.765	8.21	-5.73	-7.76	VALD
1	3933.661	0.000	-2.084	8.21	-5.73	-7.76	VALD
1	3933.664	0.000	+0.092	8.21	-5.73	-7.76	VALD
3	6162.173	1.899	+0.100	7.82	-5.07	-7.59	KB

Note.

The first four columns are self-explanatory. The damping parameters are given in the following three columns:

Gammar is the radiation damping width (s^{-1}), $\log \gamma_{\text{rad}}$.

Gammas is the Stark damping width (s^{-1}) per electron density (cm^{-3}) at 10^4 K, $\log(\gamma_e/N_e)$.

Gammaw is the van der Waals damping width (s^{-1}) per hydrogen density (cm^{-3}) at 10^4 K, $\log(\gamma_w/N_H)$.

KB ... Kurucz and Bell's (1995) compilation, VALD ... VALD database (Ryabchikova et al. 2015)

Note that Ca II 3934 line was treated as a single line (with the gf -weighted mean parameters of $\lambda = 3933.664$ Å and $\log gf = +0.105$) in the evaluation of equivalent width by using Kurucz's (1993) WIDTH9 program, since the differences between the components (corresponding to different isotopes) are negligible ($\lesssim 0.01$ Å) compared to the intrinsic stellar line width.

Table 3. NLTE abundance corrections for Ca II 3934 and Ca I 6162 lines.

Code	v_t (km s ⁻¹)	A^a (dex)	(W^{LTE}) (mÅ)	W^{NLTE} (mÅ)	A^N (dex)	A^L (dex)	Δ (dex)
[Ca II 3933.66 line]							
t070g40	2.0	6.360	(8550.67)	8609.94	6.360	6.365	-0.005
t070g40	2.0	5.360	(2703.96)	2722.70	5.361	5.366	-0.005
t070g40	2.0	4.360	(866.96)	872.97	4.360	4.367	-0.007
t085g40	2.0	6.360	(3126.08)	3147.75	6.360	6.366	-0.006
t085g40	2.0	5.360	(995.41)	1002.31	5.359	5.366	-0.007
t085g40	2.0	4.360	(345.14)	356.45	4.359	4.395	-0.036
t100g40	2.0	6.360	(805.38)	812.83	6.359	6.369	-0.010
t100g40	2.0	5.360	(297.85)	310.46	5.360	5.405	-0.045
t100g40	2.0	4.360	(167.49)	178.65	4.362	4.518	-0.156
[Ca I 6162.17 line]							
t070g40	2.0	6.360	(141.91)	164.06	6.359	6.652	-0.293
t070g40	2.0	5.360	(79.07)	84.72	5.361	5.451	-0.090
t070g40	2.0	4.360	(20.70)	18.71	4.360	4.306	+0.054
t085g40	2.0	6.360	(81.66)	92.47	6.360	6.540	-0.180
t085g40	2.0	5.360	(22.44)	20.75	5.359	5.317	+0.042
t085g40	2.0	4.360	(2.74)	2.43	4.355	4.302	+0.053
t100g40	2.0	6.360	(7.60)	7.71	6.359	6.366	-0.007
t100g40	2.0	5.360	(0.82)	0.82	5.347	5.351	-0.004
t100g40	2.0	4.360	(0.08)	0.08	4.441	4.446	-0.005

Note. Code “*taaagbb*” denotes the model (solar metallicity model with $[\text{Fe}/\text{H}] = 0.0$) with $T_{\text{eff}} = aa \times 100$ and $\log g = bb/10$. Calculations for each model were made with the microturbulence $v_t = 2 \text{ km s}^{-1}$ for three assigned Ca abundances (logarithmic number abundances in the usual normalization of $A_{\text{H}} = 12.00$): A_i^a ($\equiv 6.36 + [\text{Ca}/\text{H}]_i$) ($i = 1, 2, 3$), where $[\text{Ca}/\text{H}]_1$, $[\text{Ca}/\text{H}]_2$, and $[\text{Ca}/\text{H}]_3$ are 0.0, -1.0, and -2.0, respectively. W^{LTE} and W^{NLTE} are the resulting theoretical LTE and NLTE equivalent widths (in mÅ) corresponding to the assigned A^a , respectively. Based on such calculated non-LTE equivalent width (W^{NLTE}), two kinds of Ca abundances were inversely computed for the cases of NLTE (A^N) and LTE (A^L), from which the non-LTE abundance correction was eventually evaluated as the difference of these two, Δ ($\equiv A^N - A^L$).